TRIBOLOGY TRANSACTIONS
2017, VOL. 60, NO. 1, 95–105
http://dx.doi.org/10.1080/10402004.2016.1147629

stle
Society of Tribologists and Lubrication Engineers

Micro/Nanotexture Design for Improving Tribological Properties of Cr/GLC Films in Seawater

Yuwei Ye[a,b], Chunting Wang[a], Hao Chen[b], Yongxin Wang[a], Wenjie Zhao[a], and Yongtao Mu[c]

[a]Key Laboratory of Marine Materials and Related Technologies, Zhejiang Key Laboratory of Marine Materials and Protective Technologies, Ningbo Institute of Materials Technology and Engineering, Chinese Academy of Sciences, Ningbo, P. R. China; [b]School of Materials Science and Engineering, Jiangxi University of Science and Technology, Ganzhou, P. R. China; [c]School of Mechatronics Engineering, Harbin Institute of Technology, Harbin, P. R. China

ABSTRACT

Microdimples with different diameters and Cr/graphite-like carbon (GLC) films were fabricated on silicon by laser surface texturing and magnetron sputtering technology, respectively. The texturing effects on the microstructures and tribological performance in seawater were comparatively investigated. The results showed that both the friction coefficients and wear rates in seawater decreased with an increase in dimple diameter in the lower range and then increased with a further increase in diameter. The Cr/GLC film with an appropriate diameter of dimples (1.5 μm) is effective in enhancing the tribological properties due to entrapment of wear particles and seawater in the dimples. In addition, the roughness and graphitization contact area have obvious effects on the wear resistance. If the surface roughness is too high, the graphitization contact area will decrease, and the ratio of minimum aqueous film thickness to the surface roughness is so small that the load is almost totally borne by the boundary film.

ARTICLE HISTORY
Received 1 September 2015
Accepted 21 January 2016

KEYWORDS
Cr/GLC films; diameter of dimple; tribological properties; seawater

Introduction

With ocean exploitation occurring worldwide, there is a growing focus on the application performance of materials in an ocean environment and development of new materials suitable for an ocean environment (Wang, et al. *(1)*). Graphite-like carbon (GLC), an amorphous carbon mainly composed of sp^2-hybridized sites, was widely used in aqueous hydraulic system due to its high hardness, low residual stress, good adhesion force, and tribological properties (Wang, et al. *(2)*–*(5)*; Huang, et al. *(6)*; Ding, et al. *(7)*; Guan and Wang *(8)*; Guan, et al. *(9)*). For example, some ships, robots, motors, and pumps working in water or seawater conditions suffer damage during frequent starting/stopping or under occasional overload conditions (Ye, et al. *(10)*). However, some researchers pointed out that doping Cr, Ti, W, Mo, and Zr elements into GLC film can significantly improve the wear resistance, especially for Cr element (Camino, et al. *(11)*; Fox, et al. *(12)*; Singh, et al. *(13)*; Hovsepian, et al. *(14)*; Sheeja, et al. *(15)*; Wang, et al. *(16)*; Fu, et al. *(17)*; Uglov, et al. *(18)*). Yang and Teer *(19)* and Yang, et al. *(20)* indicated that doping an appropriate Cr element into GLC film not only improved the adhesion force but also improved the tribological performance. In a seawater environment, Shan, et al. *(21)* compared the tribological properties of a CrN single-layer coating and multilayer coating and found that the friction coefficient of the multilayer coating was lower than that of the CrN single-layer coating in seawater. Ye, et al. *(10)* researched the tribological performance of CrN and CrCN coatings in seawater and indicated that the lower friction performance of the CrCN coating was closely related to the self-lubricating amorphous carbon phase. Wang, et al. *(22)* studied the tribological performance of a Cr/GLC film coupled with Si_3N_4, SiC, WC, Al_2O_3, and ZrO_2 in seawater and reported that the friction coefficient and wear rate of the Cr/GLC film sliding against Si_3N_4 was lower than that of others. In addition, various surface modification technologies have been used to resolve the tribological problems of films. Surface texture, an artificial topography on the surface of a material, has been introduced to enhance the tribological properties of substrate material, and its antiwear and friction reducing mechanisms have been reported as a decrease in real contact area, wear debris entrapment, local increase of lubricant supply by fluid reservoirs, and increase in load-carrying capacity through a hydrodynamic effect (He, et al. *(23)*). Pettersson and Jacobson *(24)* found that a proper textured shape and size obviously enhanced the wear resistance of a diamond-like (DLC) film in an aqueous system. Wang, et al. *(25)* studied the effect of dimple area density and size on the tribological behavior of SiC in water and discovered that the load-bearing capacity of textured SiC was 2.5 times higher than that of an untextured one. Ding, et al. *(26)* indicated that a DLC film with dimple area densities of 15 and 25% showed low friction coefficients. Zum Gahr, et al. *(27)* studied the effect of texturing on the tribological behavior of ZrO in distilled water and pointed out that the friction coefficient and wear rate of surface-textured ZrO was lower than that of an untextured one.

Unfortunately, little research has been devoted to exploring the tribological properties of textured Cr/GLC films under

CONTACT Yongxin Wang yxwang@nimte.ac.cn

Color versions of one or more of the figures in the article can be found online at www.tandfonline.com/utrb.

Review led by Gary Doll

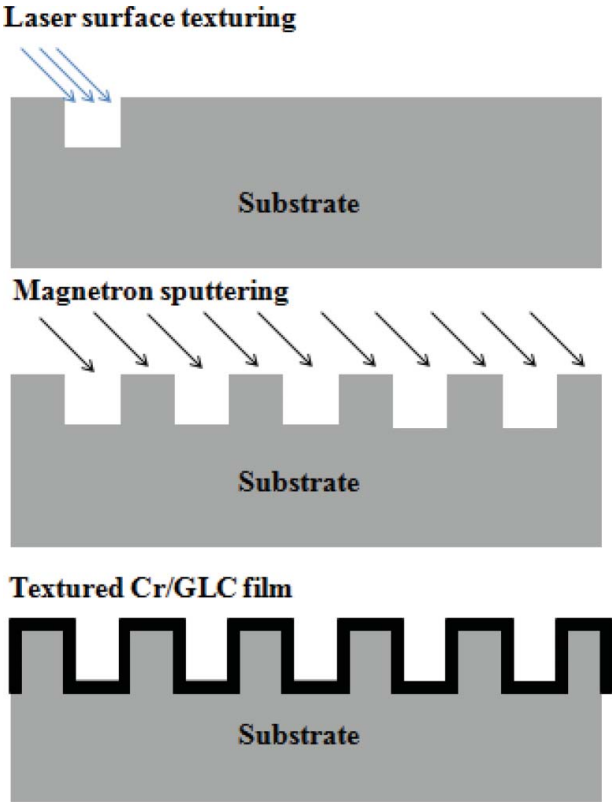

Figure 1. Schematic illustration of the process of producing textured Cr/GLC films.

seawater. Therefore, this study aims to investigate the effects of surface texture on the tribological performance of Cr/GLC films in a seawater environment. There are many surface texturing techniques, such as mechanical machining, ion beam texturing, laser texturing, and chemical etching (Koszela, et al. *(28)*; Pettersson and Jacobson *(29)*, *(30)*; Wang and Kato *(31)*; Etsion *(32)*, *(33)*; Vilhena, et al. *(34)*; Volchok, et al. *(35)*). These techniques have been developed to prepare micrometer-sized features on the surface of a material. Laser surface texturing (LST) is widely used to improve the tribological performance of films because of its versatility, fast adaptability, high precision, and cleanness of environment (He, et al. *(23)*; Zou, et al. *(36)*; Song, et al. *(37)*; Chilamakuri and Bhushan *(38)*; Sudeep, et al. *(39)*). Textured single-crystal silicon with microdimple patterns was produced by a laser system. The textured surface was strengthened using high-energy ion implantation, and the Cr/GLC films were immediately deposited by magnetron sputtering. The microstructure and tribological performance of textured and untextured Cr/GLC films were also comparatively investigated, providing better knowledge of the performance of textured Cr/GLC films. The friction process in seawater and antiwear mechanisms were investigated by probing into the effects of dimple diameter.

Experimental detail

Preparation of the GLC films with micro/nanodimples

The preparation of the GLC films with microdimples is shown in Fig. 1. There are two parts to the preparation process. Firstly, a laser surface texturing method was used to generate the surface micro/nanotextures on the silicon surface; details of the parameters are shown in Table 1. Then a thin hard Cr/GLC film with a thickness of about 3.5 μm was deposited on as-prepared single-crystal silicon substrates by magnetron sputtering. Deposition was carried out on a magnetron sputtering system (TEER, UDP650-4). Prior to deposition, all substrates were ultrasonically cleaned with acetone and ethanol for approximately 15 min. The chamber was pumped down to a background pressure less than 1×10^{-3} Pa and then the substrates were cleaned by Ar^{+} bombardment for 30 min with a bias voltage of −500 V to remove the thin oxide layer and other adherent impurities. Then, open one chromium targets (purity > 99.5 wt%, Φ 63 × 32 mm), the Cr interlayer was deposited on the substrates in advance for about 500 nm to increase the adhesion strength between the film and substrate. Deposition of the Cr interlayer was conducted for 30 min under a voltage of −70 V, a target current of 3 A, and an Ar flow rate of 16 sccm. Then Cr/GLC film deposition was performed using an Ar (purity 99.99%) flow rate of 16 sccm and a pressure of 0.5 Pa. Meanwhile, open three graphite targets and three chromium targets; the current of graphite targets and chromium targets was 3.5 and 0.38 A, respectively. The bias voltage was −70 V, the flow rate of Ar (purity 99.99%) was 16 sccm, and the deposition time was 4 h for the Cr/GLC film.

Table 1. Sample parameters (μm).

Sample	Distance	Depth	Diameter
S1	—	—	0
S2	10	1.5	0.6
S3	10	1.5	1.5
S4	10	1.5	5.5

Surface characterization

The surface morphologies of GLC films with microdimples were examined with an atomic force microscope (AFM; AIST-NT, CETR) in contact mode. The X-ray photoelectron spectroscopy (XPS) spectra were measured using an AXIS Ultra DLD XPS with an Al(mono) Kα X-ray source that was operated at 12 kV and 10 mA. The cross-section morphologies were characterized by scanning electron microscopy (SEM) using an FEI Quanta FEG 250 SEM equipped with an energy-dispersive spectroscopy (EDS) analyzer (OXFORD X-Max). The static contact angle was measured according to the sessile drop method using a contact angle analyzer (OCA20) with artificial seawater. Roughness was measured by an Alpha-Step IQ profile meter. The scanning length was 2,000 nm and six scans were performed. The scanning areas were random and contained the dimple area.

The hardness and elastic modulus were obtained from these curves using the Oliver-Pharr method (Shan, et al. *(40)*). The maximum indentation depth was 300 nm. Six indentations were made in each sample at various positions on the coating surface to produce reliable statistical results. A UMT-3MT tribometer (CETR) was used to evaluate the friction and wear characteristics of the sliding pairs. The tests were conducted in artificial seawater that was prepared according to ASTM D 1141-98 standard. The chemical composition of the artificial seawater is provided in Table 2. The sliding time,

Table 2. Composition of seawater (g/L).

Solution	NaCl	Na_2SO_4	$MgCl_2$	$CaCl_2$	$SrCl_2$
Concentration	24.53	4.09	5.20	1.16	0.025
Solution	KCl	$NaHCO_3$	KBr	H_3BO_3	NaF
Concentration	0.695	0.201	0.101	0.027	0.003

load, and frequency were set at 60 min, 10 N, and 2 Hz, respectively. The contact pressure was about 1.64 GPa. All tests were conducted at a temperature of 15 ± 3°C with a relative humidity of 45 ± 3%. The seawater was dropped onto the sample using a dropper. Three-millimeter-diameter WC balls were used in the tests as the counterparts. The formula $K = V/FS$ was used to calculate the wear ratio, where V is the wear volume (m^3), S is the total sliding distance (m), and F is the normal load (N). The wear volume V was determined by integrating the cross-sectional profile of the wear track that was profiled by a contact surface profiler. The friction contact surfaces of the WC balls were also analyzed by SEM (S4800) and Raman spectrometry (Horiba Jobin Yvon HR800). Raman spectra of the transfer layers were obtained by Raman spectroscopic (HR800) measurement using a semiconductor/YAG laser of 532 nm with a resolution of 1 cm^{-1}. The typical data acquisition time was in the range of 60 s and the spectrum was recorded in the range of 1000–2000 cm^{-1} in order to allow reliable fitting.

Results and discussion

AFM

Figure 2 shows the 2D and 3D AFM images and line cross section of microdimple-patterned Cr/GLC films obtained using the AFM (AIST-NT, CETR) in contact mode. As shown in Fig. 2, the micropatterned structures are made of parallel and ordered dimples with the same depth but changing diameter. The surface of the Cr/GLC films is smooth, which is a typical characteristic of magnetron sputtering (Wang, et al. *(2)–(4)*). Textured Cr/GLC films with different microdimple diameters from low to high are abbreviated as S1, S2, S3, and S4. The dimple distance, depth, and diameter for all of the patterned GLC films are shown in Table 1; the distance between the holes is 10 μm and the depth of dimples is 1.5 μm. The diameter of dimples for samples S2, S3, and S4 was 0.6 1.5, and 5.5 μm, respectively. The S1 film is an ordinary Cr/GLC film and was not used for texture processing.

XPS

The chemical compositions of the Cr/GLC films were observed from the XPS spectra. The content of Cr, C, and O in Cr/GLC coating is about 13.85, 80.78, and 5.37%, respectively. Because there is no obvious difference between S2, S3, and S4 films, a full scan survey, including Cr2p,

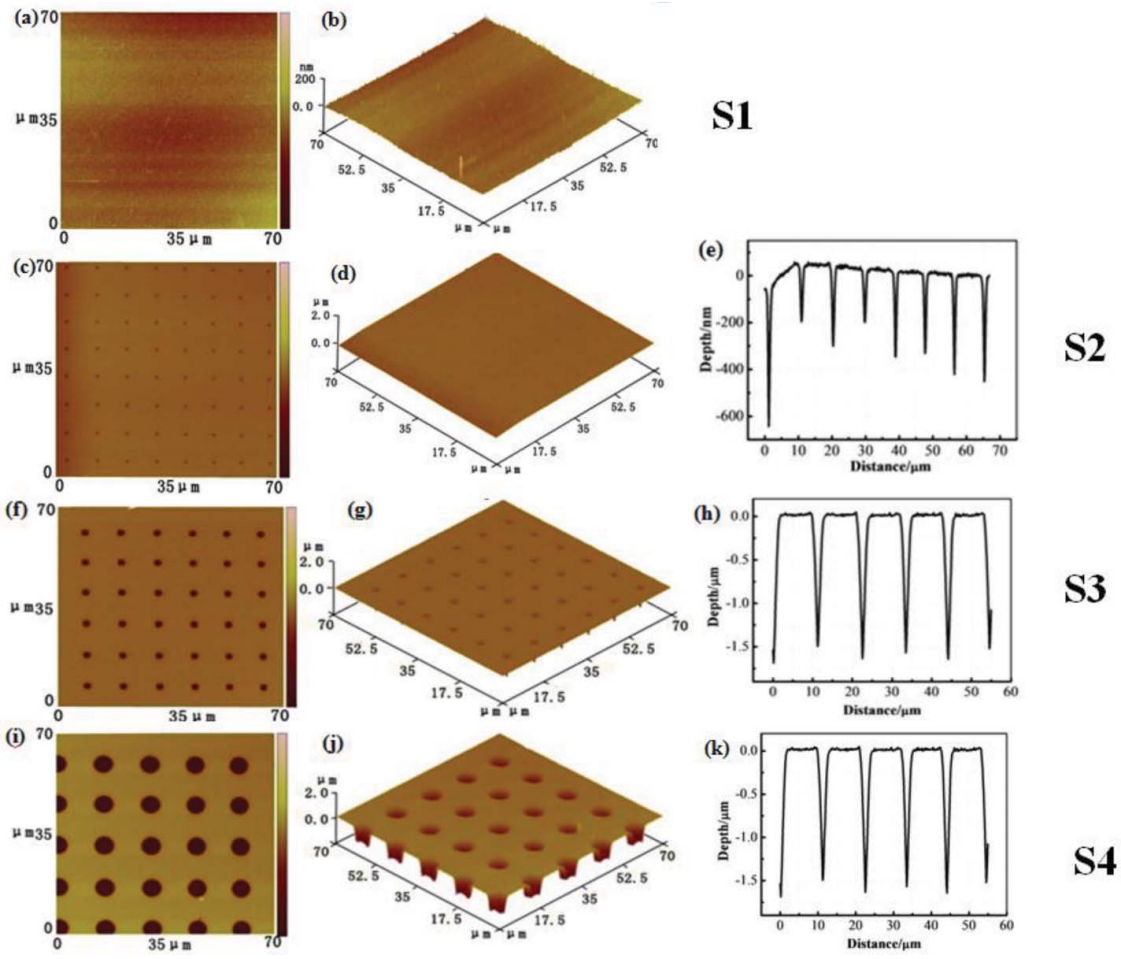

Figure 2. 2D and 3D AFM topographic images of the patterned Cr/GLC films.

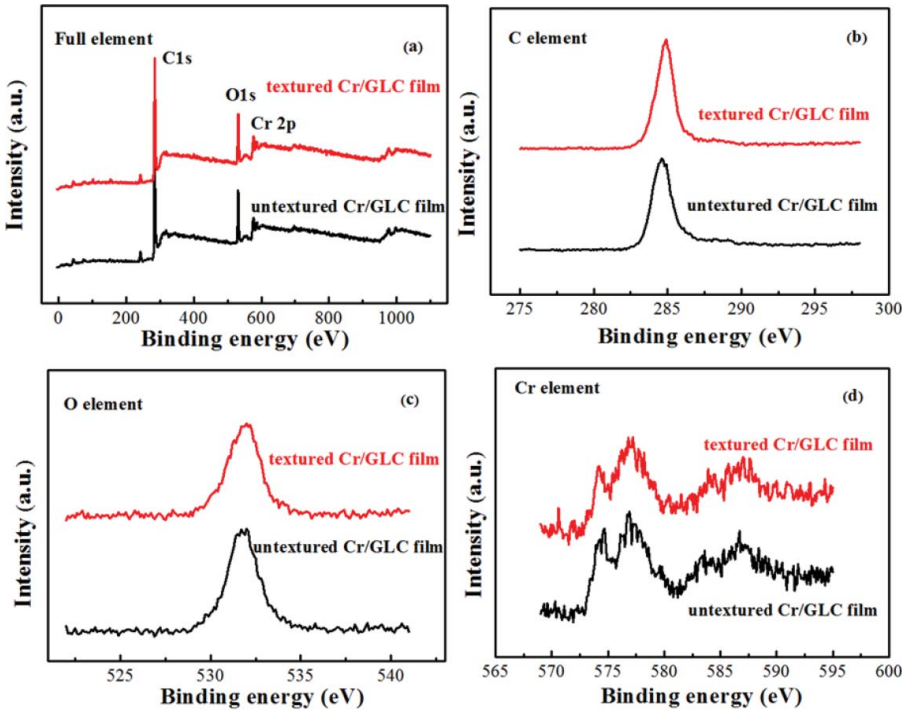

Figure 3. XPS spectra of (a) full element, (b) C1s, (c) O1s, and (d) Cr2p of the Cr/GLC films with different micro/nanotextures.

C1s, and O1s XPS spectra of the S1 and S4 films, is shown in Fig. 3. Figure 3a clearly shows the characteristic elements Cr2p, C1s, and O1s of both films, which indicated that the coating mainly contained Cr, C, and O elements. As seen in Fig. 3b, the peak of C1s at 284.8 eV correspond to an sp^2C-C bond (Dai, et al. *(41)*). The peak of O1s at 532 eV corresponding to the O=C bond is displayed in Fig. 2c (Bismarck, et al. *(42)*). In Fig. 3d, there are four prominent peaks in the Cr2p XPS spectrum, which are centered at 574.2, 578.5, 583.6, and 586.4 eV, corresponding to Cr_7C_3, Cr_2O_3, Cr_7C_3, and Cr_2O_3, respectively (Healy, et al. *(43)*; Philippe and Mark *(44)*; Halada and Clayton *(45)*; Tandon, et al. *(46)*), but these phases are stable and showed no obvious change. This indicates that texture processing did not change the chemical compositions of the films. In addition, Cr_7C_3 is a strengthening phase (Ye, et al. *(10)*; Yang and Teer *(19)*). This means that chemical reaction between Cr and C elements occurred in the deposition process, which led to the generation of a new phase.

SEM

The cross-section morphologies of the textured and untextured Cr/GLC films were observed by SEM. Similar to the XPS spectra, there is no obvious difference between S2, S3, and S4 films; the cross-section morphologies of S1 and S4 films are shown in Fig. 4. As shown in Fig. 4a, the Cr/GLC film deposited on the untextured substrate shows a dense microstructure, and the total thickness of the film is about 3.4 μm, including 0.5 μm of a pure Cr interlayer. The textured Cr/GLC film that has obvious microdimples also shows a compact structure and is well attached to the interface (Fig. 4b). The depth of the dimple is about 1.3 μm and the texture area is obvious. In addition, the GLC film has an amorphous structure under normal circumstances but a columnar structure is shown in Fig. 4, which is due to Cr doping into the GLC film, which changes the crystal growth (Yang and Teer *(19)*; Ye, et al. *(47)*). It can also be observed that S1 and S4 films show a columnar structure, which indicates that texture processing did not change the

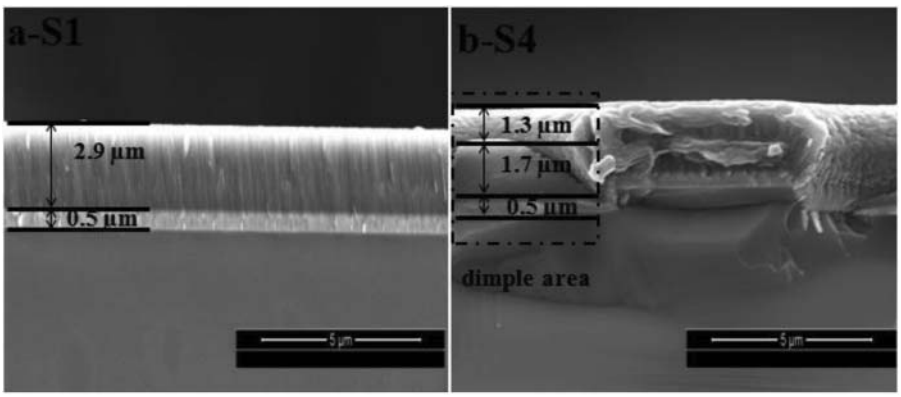

Figure 4. Cross-section morphologies of the S1 and S4 films.

Table 3. Roughness and thickness of the Cr/GLC films.

Sample	S1	S2	S3	S4
Roughness (nm)	9.05	25.6	33.8	211
Thickness (μm)	3.4	3.5	3.43	3.52

crystal growth. The roughness and thickness of the Cr/GLC films are shown in Table 3; the thickness of these films is similar, which indicates a similar deposition rate. In addition, with an increase in dimple diameter, the roughness of the Cr/GLC films shows an increasing trend, where the maximum roughness reaches its highest value at about 211 nm.

Mechanical performance

The hardness and modulus of the S1 film with a maximum indentation depth of 300 nm is shown in Fig. 5. The hardness and modulus increase significantly with an increase in indentation depth in the lower range, whereas they are constant when the indentation depth increases. According to the literature (Stan, et al. *(48)*), in order to measure the hardness of hard coatings on softer substrates, the maximum indentation depth must not exceed 10% of the thickness of the coating because above this value, plastic deformation occurs in the softer substrate. The nanoindentation test is a loading procedure, and the hardness near the surface area exist big error. Thus, the hardness and modulus are about 12 and 175 GPa, respectively.

Tribological performance

Figure 6a shows the friction curves of the textured and untextured films sliding against WC balls in seawater. The friction coefficient under seawater has similar features. As a whole, the first part shows that the friction coefficient increases to a maximum in a short time; the second part shows an obvious decrease and then a relatively steady-state wear stage is attained. The first part represents a run-in period with a rapid increase in the friction coefficient, and the second part is the rapid wear stage with an unstable friction coefficient. The decrease after the run-in period arises from a rapid increase in

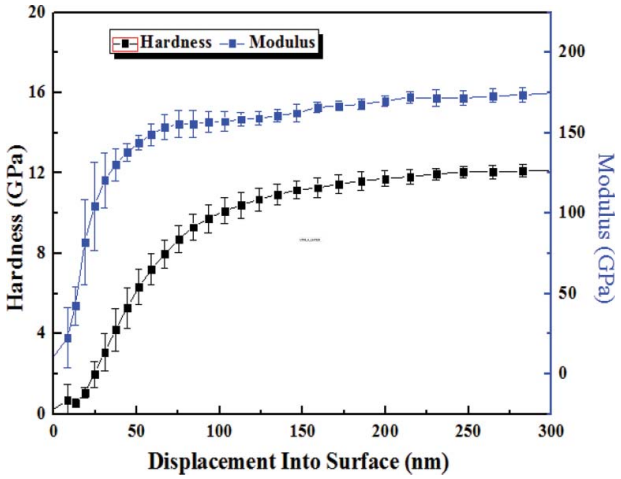

Figure 5. Evolution of the hardness and elastic modulus as a function of indentation depth for the Cr/GLC film.

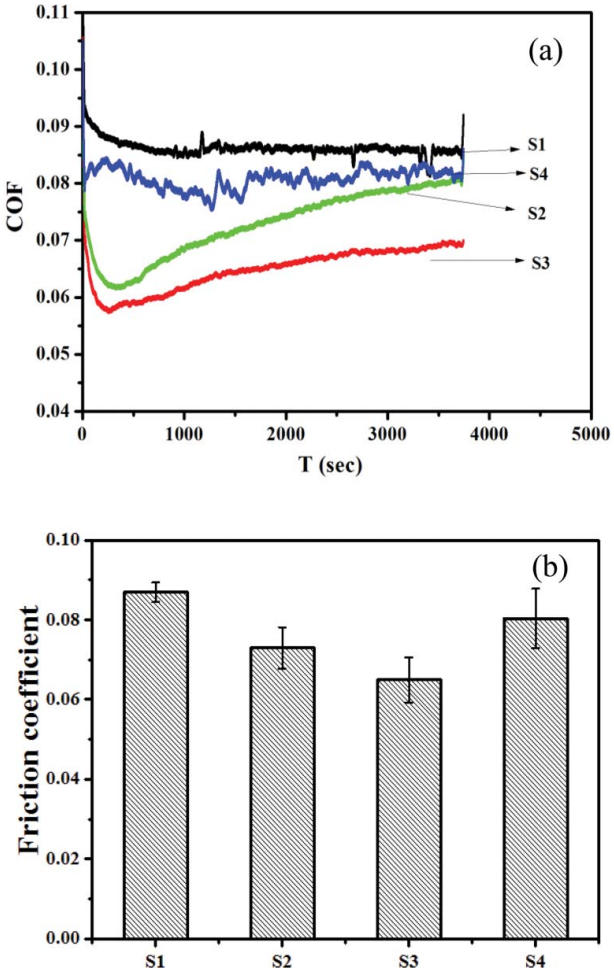

Figure 6. Friction curves and average friction coefficient of the patterned Cr/GLC films under seawater.

wear of the ball and film, which causes the interface between the tribopairs to become smoother. Moreover, continuous removal of the tribopair by sliding creates extremely smooth surfaces and the water compressed by the ambient provides hydrodynamic lubrication. In addition, the friction coefficient of textured films shows a slight increase over time due to the texture processing, which increases the roughness of the films. For the S1 film, the friction curve is very steady, indicating that the smooth surface resulted in a stable friction coefficient. Figure 6b shows the average friction coefficient of the Cr/GLC films. Due to the low viscosity of water, the lubrication regime is mixed or boundary lubrication. The comprehensive friction coefficient is determined by Eq. [1] (Ding, et al. *(26)*):

$$F = A_1 B_1 + A_2 B_2. \quad [1]$$

In this equation, A_1 is the friction coefficient, B_1 is the load-bearing ratio of the aqueous film, and A_2 and B_2 are the friction coefficient and load bearing ratio of the boundary film, respectively. As shown in Table 3, the roughness of the Cr/GLC films increased with an increase in dimple diameter. The ratio of minimum lubricant film thickness and lubrication states is close to the surface roughness. Ding, et al. *(26)* pointed out that surface texturing was effective to reduce the friction coefficient. It can be seen that the textured films show a lower friction coefficient than the untextured

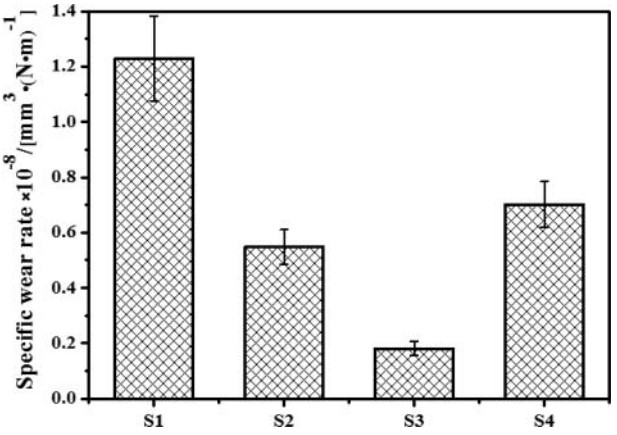

Figure 7. Wear rates of the patterned Cr/GLC films under seawater.

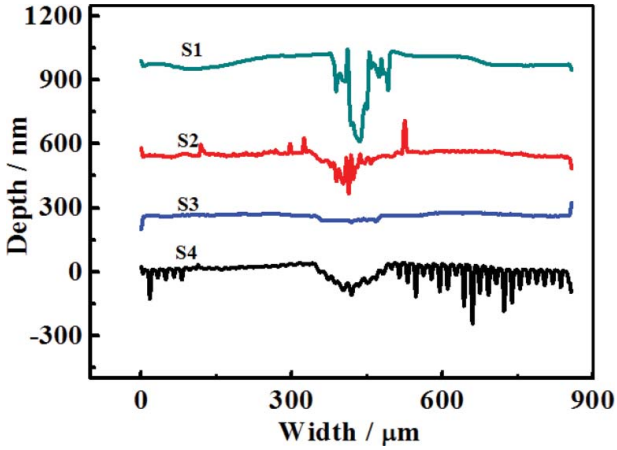

Figure 8. 2D cross-section profiles of the wear tracks on the patterned Cr/GLC films in seawater.

film (S1 sample) in seawater because the high Hertzian contact stress caused by the decrease of the real contact area contributed to the running-in of friction pairs. On the other hand, the low friction coefficient can be attributed to the trapping of some graphitization debris and seawater in the dimples. This trapping can be confirmed by the even and intact transfer layer on the counterpart sliding against the friction pair. A suitable surface roughness would be helpful for the formation of lubrication film, which plays an important role in reducing the friction coefficient. With an increase in dimple diameter, the graphitization debris produced during the friction process can be effectively trapped in the dimples. Thus, the S3 film shows a lower friction coefficient than the S2 film in seawater. However, the S4 film produced a higher friction coefficient than the S1 and S2 films because the surface roughness is too large and the ratio of minimum aqueous film thickness to the surface roughness is so small that the load is almost totally borne by the boundary film. The wear rates of the textured and untextured films are presented in Fig. 7. With an increase in dimple diameter, the wear rates of the films show a descending trend until 1.5 μm; however, when the dimple diameter further increases, the wear rates show an ascending trend. In addition, the wear rates of the textured films are lower than that of the untextured film, which is attributed to the lubricating effect of some tribochemical products (Field, et al. *(49)*). The graphitization debris is stored in the dimples, which also plays a role in lubrication. A proper surface textured can significantly improve the wear resistance of the film. This can be attributed to the extra hydrodynamic effects caused by a diminished surface texture due to the reducing thickness of the elastohydrodynamic water film under high normal load (Ding, et al. *(26)*). Seawater is a corrosive media and the wear rates of the textured films should have been higher than that of the untextured film because the dimples can store large amounts of seawater, but this was not observed, which indicates that surface texturing can enhance the wear resistance of the Cr/GCL film in seawater.

In order to further analyze the wear mechanism, the 2D cross-sectional profiles of the wear tracks of textured and untextured films are shown in Fig. 8. The S1 film shows the largest maximum depth of about 360 nm among all samples. With the increased dimple diameter, the bottom of the wear track becomes flatter, and the maximum depths show a decreasing trend until 1.5 μm, where the maximum depth reaches its lowest value at about 50 nm. However, when the dimple diameter further increases, the maximum depths show an increasing trend. The maximum wear depth of the S4 film is higher than that of films S2 and S3 in seawater, which indicates serious wear. The width of the wear track of the S1 film is about 140 μm; with increased dimple diameter, the width of the wear track shows a decreasing trend until 1.5 μm, where the width reaches its lowest value at about 115 μm. However, when the dimple diameter further increases, the widths show an increasing trend. It is worth mentioning that the maximum depth of the wear tracks on these films is lower than that of the thickness, which means that all films did not fail in seawater.

The morphologies of the wear tracks on textured and untextured films in seawater are shown in Fig. 9. It is clear that the Cr/GLC films show slight wear. As shown in Fig. 9a, the wear track of the S1 film is smooth and flat in seawater, some debris is transferred to the edge of the wear track, and there are no obvious corrosion phenomena in the wear track. Under repetitive sliding action, the asperities on the sliding surface of these films are sufficiently deformed or ploughed off to form a smoother interface. Some asperities yielded under contact stress and transferred to the edge of the wear track under shear stress. When the diameter of the dimples increased to 0.6 μm, some white debris was observed on the wear track of the S2 film (Fig. 9b). It is obviously that this large white debris cannot effectively drop into the dimples due to their size. EDS analysis showed that the white debris is mainly composed of Cr, C, O, Ca, Na, and S elements. Cr and C elements derive from the S2 film, whereas Ca, Na, and S elements derive from seawater. The EDS analysis also shows that O element exists on the surface of the wear track, indicating that oxidation occurred during sliding. When the diameter of the dimples increased to 1.5 μm, there was some debris in the wear track of the S3 film (Fig. 9c). Compared to the debris in Fig. 9b, the content of C element shows an increase trend, but the Mg and S elements show an decreasing trend, which indicates that the white debris mainly consists of salt from seawater. In Fig. 9d, the wear track is smooth and flat in seawater conditions and some wear debris particles can be observed in the dimples. The Raman spectra obtained from the contact surface of the WC balls are illustrated in Fig. 10. For sliding in seawater, a peak around at 1580 cm^{-1} can be seen, which indicates that some sp^2-hybrized carbons with a graphite structure existed in the Cr/GLC films. Because the graphite-like structure with sp^2-hybrized carbon in Cr/GLC films can act as an interface

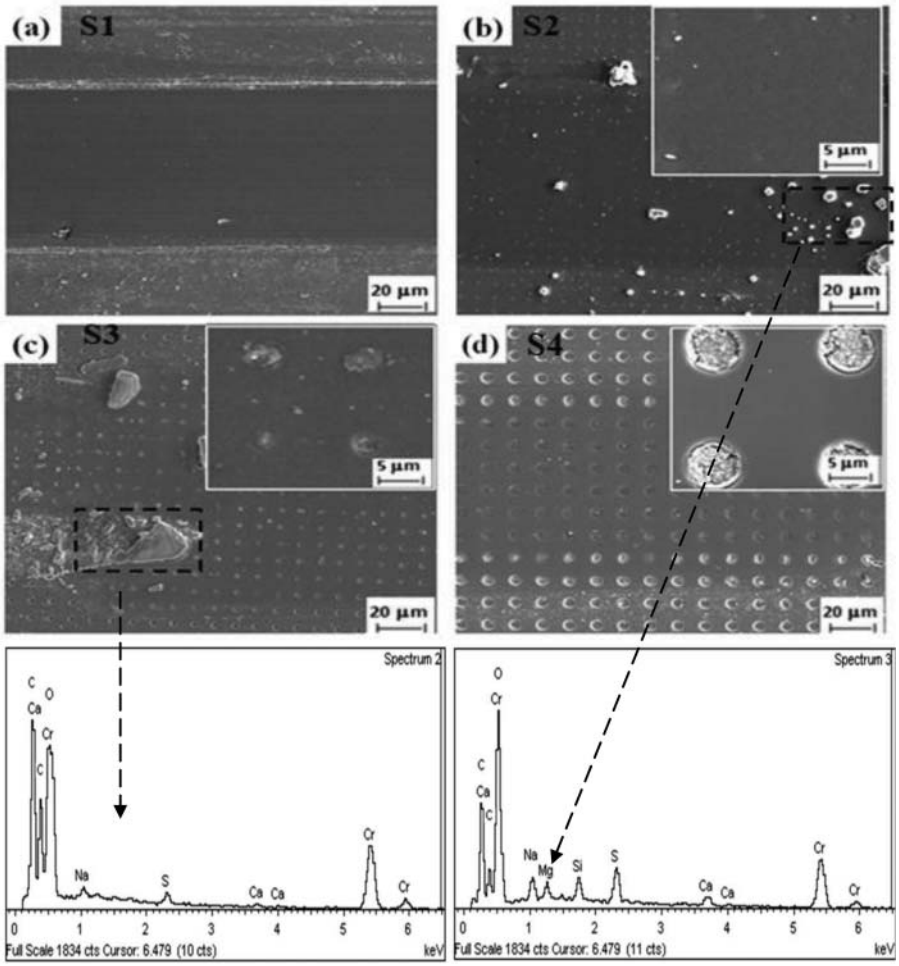

Figure 9. Morphologies of the wear tracks on the patterned Cr/GLC films in seawater.

layer during friction testing, it can significantly decrease the resistance in the tribotest. The lubricating mechanisms of sp^2-hybrized carbon can be described as follows: the sp^2-hybrized carbon with a graphite-like structure in the surface will reduce dangling σ bonds on the clean surface, which can avoid the strong adhesive phenomenon between the counterpart and film, resulting in the low surface energy of Cr/GLC-coated substrates (Wang, et al. *(50)*). In addition, the frictional shear resistance during sliding tests is reduced due to the decrease in surface energy of contacting faces (Zhang, et al. *(51)*). Moreover, the shear will induce graphitization, which can form some graphite lubricating transfer films on the surface of mating counterparts, effectively decreasing the friction coefficient (Holmberg, et al. *(52)*; Suzuki, et al. *(53)*; Sánchez-López, et al. *(54)*). In addition the low friction, the wear loss of the film is reduced obviously. It is further demonstrated in Fig. 10 that with increased dimple diameter, the intensity of the sp^2-hybrized peak shows an increasing trend until 1.5 μm, and with a further increase in dimple diameter, the intensity of the sp^2-hybrized peak shows a decreasing trend. This phenomenon is consistent with the results for the wear rate (Fig. 7). A peak of sp^3 around at 1350 cm^{-1} can be seen in this image; the intensity of the sp^3 peak increased significantly with an increase of diameter from 0 to 1.5 μm.

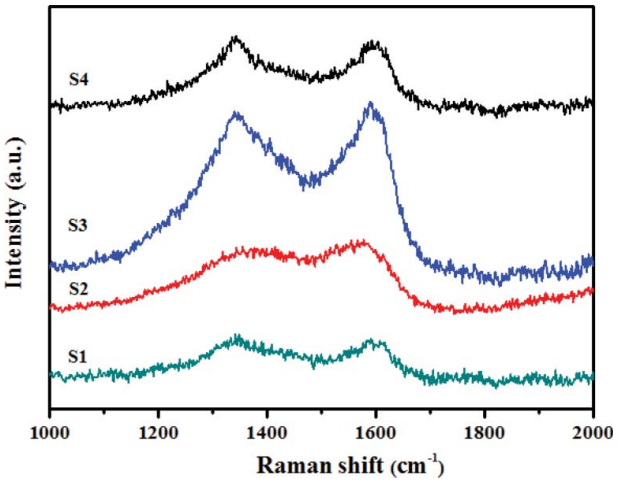

Figure 10. Raman spectra obtained from the contact surface of the WC ball.

Figure 11 shows the effect of surface texture on the contact angle of the Cr/GLC films deposited on a single-crystal silicon substrate. It is clear from Fig. 11 that with an increase in dimple diameter, the contact angles show a decreasing trend until 1.5 μm, where the contact angle reaches its lowest value at about 91.75°. However, when the dimple diameter further increases, the contact angles show an increasing trend. The contact angle of the S1 film is the largest among these films, which indicates that surface texturing can improve the hydrophilicity of the film. This is because the surface texturing provides enough dimples so that seawater is easily trapped in the

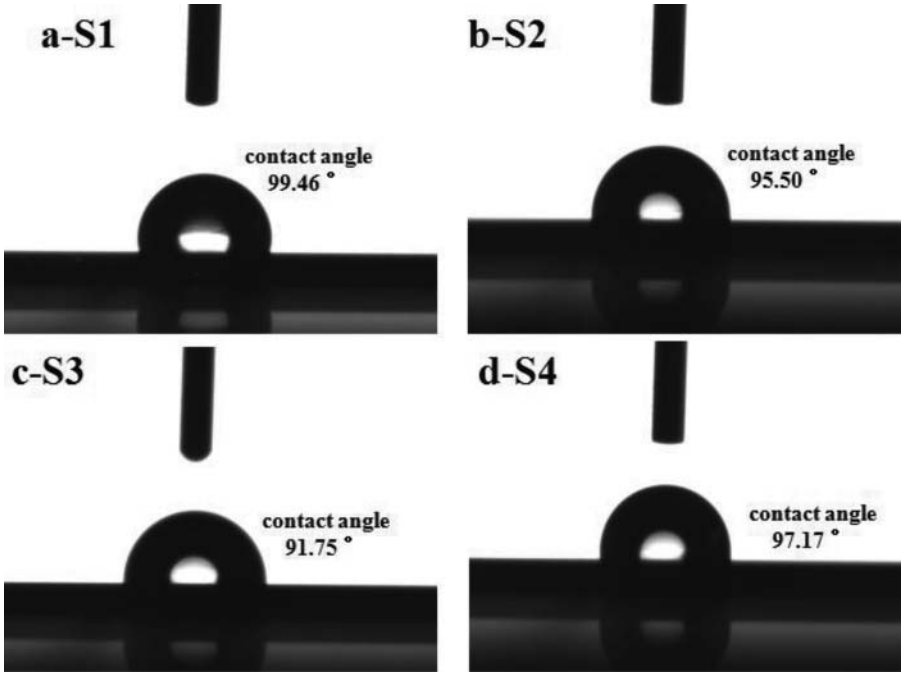

Figure 11. Effect of surface texture on the contact angle of the patterned Cr/GLC films.

dimples. Furthermore, the contact angle of the S3 film is lower than the others, which means that seawater stays on the material surface and plays a role in lubrication. Because seawater is a weak alkaline solution, Ca^{2+} and Mg^{2+} will be deposited on the counterface in the form of $Mg(OH)_2$ and $CaCO_3$ (reactions [2], [3], and [4]), which with sludge-like matter deposited on the sliding surfaces has some lubricating effect (Ye, et al. *(10)*). In addition, the contact of S4 is larger than that of samples S2 and S3, because some air is stored in the dimple between the film and droplet and increases the contact angle (Cheng, et al. *(55)*).

$$Mg^{2+} + 2H_2O \rightarrow Mg(OH)_2 + 2H^+ \quad [2]$$

$$HCO_3^- \rightarrow CO_3^{2-} + H^+ \quad [3]$$

$$Ca^{2+} + CO_3^{2-} \rightarrow CaCO_3. \quad [4]$$

To sum up, there are three key factors that affect the tribological properties of the Cr/GLC film in the tribotest: lubricant substance, surface roughness, and corrosion. According to the literature (Wang, et al. *(56)*; Yamamoto and Matsukado *(57)*; Zum Gahr, et al. *(58)*), in sliding under water-lubricated conditions, the kinematic viscosity of water is low, and it is difficult for a continuous thin fluid water film to form between the Cr/GLC film and counterpart. Therefore, it is reasonable that the tribotest in water-lubricated condition must be assigned to the mixed regime, including partial water-lubricated regions and solid–solid contact regions at the microscale (Schmidt, et al. *(59)*; Nogueira, et al. *(60)*). The surface texturing process significantly reduces the solid–solid contact regions in the cycle friction process due to seawater trapped in the dimple. The friction coefficients and wear rates in solid–solid contact regions are higher than that in water-lubricated regions, which means that the friction coefficients and wear rates of textured films are lower than those of untextured films in general. Thus, the area of water-lubricated regions in the friction test is important. In addition, graphitization debris is captured in the dimples, which can improve the tribological performance of the Cr/GLC films. Second, surface texturing increases the surface roughness indirectly during the friction test. Higher roughness reduces the actual contact area between the counterpart and film, which results in the load only focusing on the contact areas, thus enhancing the friction coefficient of the film (Riyadh, et al. *(61)*). Third, the high Cl^- ion concentration in seawater has a strong destructive effect on the Cr/GLC films. It could be easily disintegrated or removed by the action of the rapid triboball during sliding, producing a track of clean surfaces exposed to a corrosive environment. In addition, the high Cl^- ion concentration inhibits the formation of a passivation film and exposes the new surface, inducing serious corrosion and accelerating wear. The increased wear rate induces more defects and accelerates corrosion (Ye, et al. *(10)*). Figure 12 illustrates the effects of surface texturing and the Cr/GLC film on the friction and wear behavior in seawater. As shown in Fig. 12a, for the S1 film, some large hard debris stacked above the wear track interfered with the sliding friction and led to abrasive wear. The untextured film surface was not able to store seawater and lubrication particles. Most of graphitization particles are transferred to the edge of wear track. Thus, the wear rate of the S1 film is higher than the others. Figure 12b is different from Fig. 12a; that is, with increased dimple diameter, the dimples can store hard debris, graphitization particles, and seawater, thus enhancing the area of water-lubricated regions, which can slightly improve the friction and wear behavior. However, the surface roughness of the S2 film (25.6 nm) is higher than that of the S1 film (9.05 nm), which will slightly aggravate wear. Comparing Figs. 6 and 7, the friction coefficients and wear rates of the S2 film are lower than that of the S1 film, indicating that the lubrication substance (seawater and graphitization particles) plays a leading role. In Fig. 12c, when the diameter of the dimples further increases, the hard debris, graphitization particles, and seawater become trapped in the dimples and can effectively

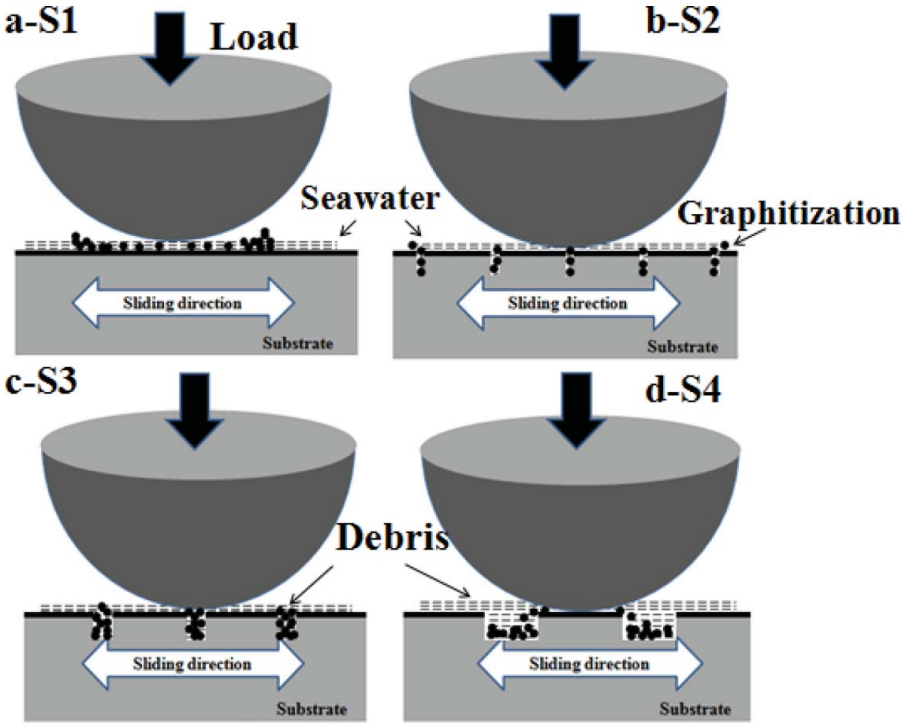

Figure 12. Cross-sectional schematic view of the wear mechanism model for (a) S1, (b) S2, (c) S3, and (d) S4.

improve the wear behavior. As shown in Fig. 12d, for the S4 film, because the diameter is too large, a large number of graphitization particles are trapped in the dimples, which prevents contact with the friction interlayer and thus does not play an obvious role in lubrication. In addition, because the surface roughness is too high, the thickness of the aqueous film is decreased and resistance during the friction test increases. Finally, seawater is trapped in the dimples, which causes serious corrosive wear. According to the results of the tribotests, roughness and corrosion play a leading role. Based on the above results, the S2 and S3 films show better overall performance in seawater, indicating their potential application as protective coatings for automotive tribocomponents.

Conclusions

The aim of this article is to investigate the effect of surface texturing on the structure and tribological properties of Cr/GLC films under seawater condition. Special attention is focused on the cross-sectional profiles of the wear tracks, the morphologies of wear tracks on tribological behaviors of textured and untextured films. Ordered Cr/GLC films with microdimple-patterned surfaces were fabricated by a combination of ICP and magnetron sputtering. In seawater, the textured film showed a lower wear rate than that of the untextured one (1.23×10^{-8} mm/Nm). This finding can be explained by the lubrication of seawater stored in the dimples. A proper surface roughness will aid in the formation of a lubrication film and the hard particles trapped in the dimples, which increase the graphitization contact area between the film and friction pair. In addition, the S3 film exhibited the lowest friction coefficient (0.065) and wear rate (1.94×10^{-9} mm/Nm) among these samples, indicating its potential application in the design and selection of appropriate micro/nanopattern parameters for automotive tribocomponents in seawater.

Funding

This work was supported by the National Natural Science Foundation of China (Grant Nos. 51202263, 51161008, 51202261, and 51475449) and the National Basic Research Program of China (973 Program, Grant No. 2013CB632302).

References

(1) Wang, J. Z., Yan, F. Y., and Xue, Q. J. (2009), "Friction and Wear Behavior of Ultra-High Molecular Weight Polyethylene Sliding against GCr15 Steel and Electroless Ni-P Alloy Coating under the Lubrication of Seawater," *Tribology Letters*, **35**, pp 85–95.

(2) Wang, Y. X., Wang, L. P., Li, J. L., Chen, J. M., and Xue, Q. J. (2013), "Tribological Properties of Graphite-Like Carbon Coatings Coupling with Different Metals in Ambient Air and Water," *Tribology International*, **60**, pp 147–155.

(3) Wang, Y. X., Li, J. L., Wang, L. P., Chen, J. M., and Xue, Q. J. (2013), "Tribological Performances of Graphite-Like Carbon Films Coupled to Different Ceramics in Ambient Air and Water," *Tribology Transactions*, **56**, pp 333–341.

(4) Wang, Y. X., Wang, L. P., and Xue, Q. J. (2011), "Controlling Wear Failure of Graphite-Like Carbon Film in Aqueous Environment: Two Feasible Approaches," *Applied Surface Science*, **257**, pp 4370–4376.

(5) Huang, J. X., Wan, S. H., Wang, L. P., and Xue, Q. J. (2015), "Tribological Properties of Si-Doped Graphite-Like Amorphous Carbon Film of PEEK Rubbing with Different Counterparts in SBF Medium," *Tribology Letters*, **57**, pp 10–18.

(6) Huang, J. X., Wang, L. P., Li, B., Wan, S. H., and Xue, Q. J. (2015), "In vitro Evaluation of the Tribological Response of Mo-Doped Graphite-Like Carbon Film in Different Biological Media," *ACS Applied Materials & Interfaces*, **7**, pp 2772–2783.

(7) Ding, Q., Wang, L. P., Hu, L. T., Hu, T. C., and Wang, Y. (2012), "The Pairing-Dependent Effects of Laser Surface Texturing on Micro Tribological Behavior of Amorphous Carbon Film," *Wear*, **274–275**, pp 43–49.

(8) Guan, X. Y. and Wang, L. P. (2012), "The Tribological Performances of Multilayer Graphite-Like Carbon (GLC) Coatings Sliding against

Polymers for Mechanical Seals in Water Environments," *Tribology Letters*, **47**, pp 67–78.
(9) Guan, X. Y., Lu, Z. B., and Wang, L. P. (2011), "Achieving High Tribological Performance of Graphite-Like Carbon Coatings on Ti6Al4V in Aqueous Environments by Gradient Interface Design," *Tribology Letters*, **44**, pp 315–325.
(10) Ye, Y. W., Wang, Y. X., Chen, H., Li, J. L., Yao, Y. R., and Wang, C. T. (2015), "Doping Carbon to Improve the Tribological Performance of CrN Coatings in Seawater," *Tribology International*, **90**, pp 362–371.
(11) Camino, D., Jones, A. H. S., Mercs, D., and Teer, D. G. (1999), "High Performance Sputtered Carbon Coatings for Wear Resistant Applications," *Vacuum*, **52**, pp 125–131.
(12) Fox, V., Jones, A., Renevier, N. M., and Teer, D. G. (2000), "Hard Lubricating Coatings for Cutting and Forming Tools and Mechanical Components," *Surface and Coatings Technology*, **125**, pp 347–353.
(13) Singh, V., Jiang, J. C., and Meletis, E. I. (2005), "Cr-Diamond Like Carbon Nanocomposite Films: Synthesis, Characterization and Properties," *Thin Solid Films*, **489**, pp 150–158.
(14) Hovsepian, P. E., Lewis, D. B., Constable, C., Luo, Q., Kok, Y. N., and Munz, W. D. (2003), "Combined Steered Cathodic Arc/Unbalanced Magnetron Grown C/Cr Nanoscale Multilayer Coatings for Tribological Applications," *Surface and Coatings Technology*, **174–175**, pp 762–769.
(15) Sheeja, D., Tay, B. K., Sun, C. Q., and Fu, Y. Q. (2003), "Characterization of Ti Containing Amorphous Carbon Films Prepared on Titanium Substrate," *Journal of Materials Science*, **38**, pp 421–425.
(16) Wang, A. Y., Lee, K. P., Ahn, J. P., and Han, J. H. (2006), "Structure and Mechanical Properties of W Incorporated Diamond-Like Carbon Films Prepared by a Hybrid Ion Beam Deposition Technique," *Carbon*, **44**, pp 1826–1832.
(17) Fu, R. K. Y., Mei, Y. F., Fu, M. Y., Liu, X. Y., and Chu, P. K. (2005), "Thermal Stability of Metal-Doped Diamond-Like Carbon Fabricated Dual Plasma Deposition," *Diamond and Related Materials*, **14**, pp 1489–1493.
(18) Uglov, V. V., Kuleshov, A. K., Rusalsky, D. P., Onate, J. I., and Yang, S. Z. (2000), "Wear Resistant Metal–Carbon Composite Coating," *Surface and Coatings Technology*, **128–129**, pp 150–155.
(19) Yang, S. and Teer, D. G. (2000), "Investigation of Sputtered Carbon and Carbon/Chromium Multi-Layered Coatings," *Surface and Coatings Technology*, **131**, pp 412–416.
(20) Yang, S., Li, X., Renevier, N. M., and Teer, D. G. (2001), "Tribological Properties and Wear Mechanism of Sputtered C/Cr Coating," *Surface and Coatings Technology*, **142–144**, pp 85–93.
(21) Shan, L., Wang, Y., Li, J., Jiang, X., and Chen, J. (2015), "Architecture of Multilayer Cr/CrN Coatings for Wear Protection in Seawater: Cr/CrN Ratio and Total Thickness," *Tribology Transactions*, **58**, pp 914–923.
(22) Wang, C., Ye, Y., Guan, X., Hu, J., Wang, Y., and Li, J. (2016), "An Analysis of Tribological Performance on Cr/GLC Film Coupling with Si_3N_4, SiC, WC, Al_2O_3 and ZrO_2 in Seawater," *Tribology International*, **96**, pp 77–86.
(23) He, D. Q., Zheng, S. X., Pu, J. B., Zhan, G. A., and Hu, L. T. (2015), "Improving Tribological Properties of Titanium Alloys by Combining Laser Surface Texturing and Diamond-Like Carbon Film," *Tribology International*, **8**, pp 20–27.
(24) Pettersson, U. and Jacobson, S. (2004), "Friction and Wear Properties of Micro Textured DLC Coated Surfaces in Boundary Lubricated Sliding," *Tribology Letters*, **17**, pp 553–559.
(25) Wang, X., Kato, K., Adachi, K., and Aizawa, K. (2014), "Loads Carrying Capacity Map for the Surface Texture Design of SiC Thrust Bearing Sliding in Water," *Tribology International*, **36**, pp 189–197.
(26) Ding, Q., Wang, L., Wang, Y., Wang, S. C., Hu, L. and Xue, Q. (2010), "Improved Tribological Behavior of DLC Films under Water Lubrication by Surface Texturing," *Tribology Letters*, **41**, pp 439–449.
(27) Zum Gahr, K. H., Mathieu, M., and Brylka, B. (2007), "Friction Control by Surface Engineering of Ceramic Sliding Pairs in Water," *Wear*, **263**, pp 920–929.
(28) Koszela, W., Pawlus, P., and Galda, L. (2007), "The Effect of Oil Pockets Size and Distribution on Wear in Lubricated Sliding," *Wear*, **263**, pp 1585–1592.
(29) Pettersson, U. and Jacobson, S. (2007), "Friction and Wear Properties of Micro Textured DLC Coated Surfaces in Boundary Lubricated Sliding," *Tribology International*, **40**, pp 355–359.
(30) Pettersson, U. and Jacobson, S. (2003), "Influence of Surface Texture on Boundary Lubricated Sliding Contacts," *Tribology International*, **36**, pp 857–864.
(31) Wang, X. and Kato, K. (2002), "Improving the Anti-Seizure Ability of SiC Seal in Water with RIE Texturing," *Tribology Letters*, **14**, pp 275–280.
(32) Etsion, I. (2004), "Improving Tribological Performance of Mechanical Components by Laser Surface Texturing," *Tribology Letters*, **17**, pp 733–737.
(33) Etsion, I. (2005), "State of the Art in Laser Surface Texturing," *Journal of Tribology*, **127**, pp 248–253.
(34) Vilhena, L. M., Sedlaček, M., Podgornik, B., Vižintin, J., Babnik, A., and Možina, J. (2009), "Surface Texturing by Pulsed Nd:YAG Laser," *Tribology International*, **42**, pp 1496–1504.
(35) Volchok, A., Halperin, G., and Etsion, I. (2002), "The Effect of Surface Regular Microtopography on Fretting Fatigue Life," *Wear*, **253**, pp 509–515.
(36) Zou, M., Cai, L., and Yang, D. (2006), "Nanotribology of a Silica Nanoparticle-Textured Surface," *Tribology Transactions*, **49**, pp 66–71.
(37) Song, H., Ji, L., Li, H., Liu, X., Zhou, H., Liu, L., and Chen, L. (2015), "Superlow Friction Behavior of Surface-Textured a-C:H Film in Water Environments," *Tribology Transactions*, **58**, pp 867–874.
(38) Chilamakuri, S. K. and Bhushan, B. (1997), "Optimization of Asperities for Laser-Textured Magnetic Disk Surfaces," *Tribology Transactions*, **40**, pp 303–311.
(39) Sudeep, U., Tandon, N., and Pandey, R. K. (2015), "Tribological Studies of Lubricated Laser-Textured Point Contacts in Rolling/Sliding Reciprocating Motion with Investigations of Wettability and Nanohardness," *Tribology Transactions*, **58**, pp 625–634.
(40) Shan, L., Wang, Y., Li, J., Li, H., Wu, X., and Chen, J. (2013), "Tribological Behaviours of PVD TiN and TiCN Coatings in Artificial Seawater," *Surface and Coatings Technology*, **226**, pp 40–50.
(41) Dai, W., Ke, P. L., and Wang, A. Y. (2011), "Microstructure and Property Evolution of Cr-DLC Films with Different Cr Content Deposited by a Hybrid Beam Technique," *Vacuum*, **85**, pp 792–797.
(42) Bismarck, A., Tahhan, R., Springer, J. S. A., Schulz, A., Klapötke, T. M., Zeil, H., and Michaeli, W. (1997), "Influence of Fluorination on the Properties of Carbon Fibres," *Journal of Fluorine Chemistry*, **84**, pp 127–134.
(43) Healy, M. D., Smith, D. C., Rubiano, R. R., Elliott, N. E., and Springer, R. W. (1994), "Use of Tetraneopentylchromium as a Precursor for the Organometallic Chemical Vapor Deposition of Chromium Carbide: A Reinvestigation," *Chemistry of Materials*, **6**, pp 448–453.
(44) Philippe, M. and Mark, E. B. (1992), "XPS Study of the Passive Films Formed on Nitrogen-Implanted Austenitic Stainless Steels," *Applied Surface Science*, **59**, pp 7–21.
(45) Halada, G. P. and Clayton, C. R. J. (1991), "Photoreduction of Hexavalent Chromium during X-ray Photoelectron Spectroscopy Analysis of Electrochemical and Thermal Films," *Journal of the Electrochemical Society*, **138**, pp 2921–2927.
(46) Tandon, R. K., Payling, R., Chenhall, B. E., Crisp, P. T., Elli, J., and Baker, R. S. (1985), "Application of X-ray Photoelectron Spectroscopy to the Analysis of Stainless-Steel Welding Aerosols," *Applied Surface Science*, **20**, pp 527–537.
(47) Ye, Y., Wang, C., Wang, Y., Zhao, W., Li, J., and Yao, Y. (2015), "A Novel Strategy to Enhance the Tribological Properties of Cr/GLC Films in Seawater by Surface Texturing," *Surface and Coatings Technology*, **280**, pp 338–346.
(48) Stan, V., Maritza, G. J., Veprek, H., Pavla, K., and Jan, P. (2005), "Different Approaches to Superhard Coatings and Nanocomposites," *Thin Solid Films*, **476**, pp 1–29.
(49) Field, S. K., Jarratt, M., and Teer, D. G. (2004), "Tribological Properties of Graphite-Like and Diamond-Like Carbon Coatings," *Tribology International*, **37**, pp 949–956.

(50) Wang, Y., Wang, L., Zhang, G., Wang, S., Wood, R. J. K., and Xue, Q. (2010), "Effect of Bias Voltage on Microstructure and Properties of Ti-Doped Graphite-Like Carbon Films Synthesized by Magnetron Sputtering," *Surface and Coatings Technology*, **205**, pp 793–800.

(51) Zhang, H. S., Endrino, J. L., and Anders, A. (2008), "Comparative Surface and Nano-Tribological Characteristics of Nanocomposite Diamond-Like Carbon Thin Films Doped by Silver," *Applied Surface Science*, **255**, pp 2551–2256.

(52) Holmberg, K., Ronkainen, H., Laukkanen, A., and Wallin, K. (2007), "Friction and Wear of Coated Surfaces—Scales, Modelling and Simulation of Tribomechanisms," *Surface and Coatings Technology*, **202**, pp 1034–1049.

(53) Suzuki, M., Tanaka, A., Ohana, T., and Zhang, W. (2004), "Frictional Behavior of DLC Films in a Water Environment," *Diamond and Related Materials*, **13**, pp 1464–1468.

(54) Sánchez-López, J. C., Erdemir, A., Donnet, C., and Rojas, T. C. (2002), "Friction-Induced Structural Transformations of Diamond Like Carbon Coatings under Various Atmospheres," *Surface and Coatings Technology*, **163–164**, pp 444–450.

(55) Cheng, S., Dong, K., and Zhang, X. (2007), "Study of the Influence of Apparent Contact Angle on Regular Rough Surface Considering Liquid Wetting Properties," *Mechanical Science and Technology for Aerospace Engineering*, **26**, pp 822–827.

(56) Wang, D., Li, Z., and Zhu, Y. (2003), "Lubrication and Tribology in Seawater Hydraulic Piston Pump," *Journal of Marine Science and Application*, **2**, pp 35–40.

(57) Yamamoto, K. and Matsukado, K. (2006), "Effect of Hydrogenated DLC Coating Hardness on the Tribological Properties under Water Lubrication," *Tribology International*, **39**, pp 1609–1614.

(58) Zum Gahr, K. H., Mathieua, M., and Brylka, B. (2007), "Friction Control by Surface Engineering of Ceramic Sliding Pairs in Water," *Wear*, **263**, pp 920–929.

(59) Schmidt, T., André, M., and Poll, G. (2010), "A Transient 2D-Finite-Element Approach for the Simulation of Mixed Lubrication Effects of Reciprocating Hydraulic Rod Seals," *Tribology International*, **43**, pp 1775–1785.

(60) Nogueira, I., Dias, A. M., Gras, R., and Progri, R. (2002), "An Experimental Model for Mixed Friction during Running-In," *Wear*, **253**, pp 541–549.

(61) Riyadh, A., Samarai, A., Haftirman , Ahmad, K. R., and Al-Douri, Y. (2013), "Effect of Roughness of Hypo- and Hyper-Eutectic Al-Si Piston Alloy on Wear Characteristics under Lubrication," *Procedia Engineering*, **53**, pp 616–623.